Molecular Diversity
https://doi.org/10.1007/s11030-020-10107-0

ORIGINAL ARTICLE

Structure-based drug design, synthesis and screening of MmaA1 inhibitors as novel anti-TB agents

Hymavathi Veeravarapu[1,2] · Vasavi Malkhed[2] · Kiran Kumar Mustyala[2] · Rajender Vadija[2] · Ramesh Malikanti[2] · Uma Vuruputuri[2] · Murali Krishna Kumar Muthyala[1]

Received: 3 April 2020 / Accepted: 15 May 2020

Abstract

Tuberculosis is one of the leading causes of death across the world. The treatment regimens for tuberculosis are well established, but still the control of the disease faces many challenges such as lengthy treatment protocols, drug resistance and toxicity. In the present work, mycolic acid methyl transferase (MmaA1), a protein involved in the maturation of mycolic acids in the biochemical pathway of the *Mycobacterium*, was studied for novel drug discovery. The homology model of the MmaA1 protein was built and validated by using computational techniques. The MmaA1 protein has 286 amino acid residues consisting of 10 α-helices and 7 β-sheets. The active site of the MmaA1 protein was identified using CASTp, SiteMap and PatchDock. Virtual screening studies were performed with two small molecule ligand databases: Asinex synergy and Diverse_Elite_Gold_Platinum databases having a total of 43,446 molecules and generated 1,30,814 conformers against the predicted and validated active site of the MmaA1 protein. Binding analysis showed that the residues ASP 19, PHE 22, TRP 30, TYR 32, TRP 74 and ALA 77 of MmaA1 protein have consistent interactions with the ligands. The hit ligands were further filtered by in silico ADME properties to eliminate potentially toxic molecules. Of the top 10 molecules, 3-(2-morpholinoacetamido)-*N*-(1,4-dihydro-4-oxoquinazolin-6-yl) benzamide was synthesised and screened for in vitro anti-TB activity against *Mtb* H37Rv using MABA assay. The compound and its intermediates exhibited good in vitro anti-TB activity which can be taken up for future lead optimisation studies.

Electronic supplementary material The online version of this article (https://doi.org/10.1007/s11030-020-10107-0) contains supplementary material, which is available to authorized users.

✉ Murali Krishna Kumar Muthyala
drmmkau@gmail.com

[1] Pharmaceutical Chemistry Research Lab, AU College of Pharmaceutical Sciences, Andhra University, Visakhapatnam, Andhra Pradesh 530003, India

[2] Molecular Modelling Research Lab, Department of Chemistry, University College of Science, Osmania University, Hyderabad, Telangana, India

Published online: 12 June 2020

Graphical abstract

Structure based virtual screening study was performed using a validated homology model against small molecules from two virtual compound libraries. Synthesised the lead compound 3-(2-morpholinoacetamido)-*N*-(1,4-dihydro-4-oxoquinazolin-6-yl)benzamide obtained from virtual screening. In vitro activity against Mtb H37Rv has given a promising result.

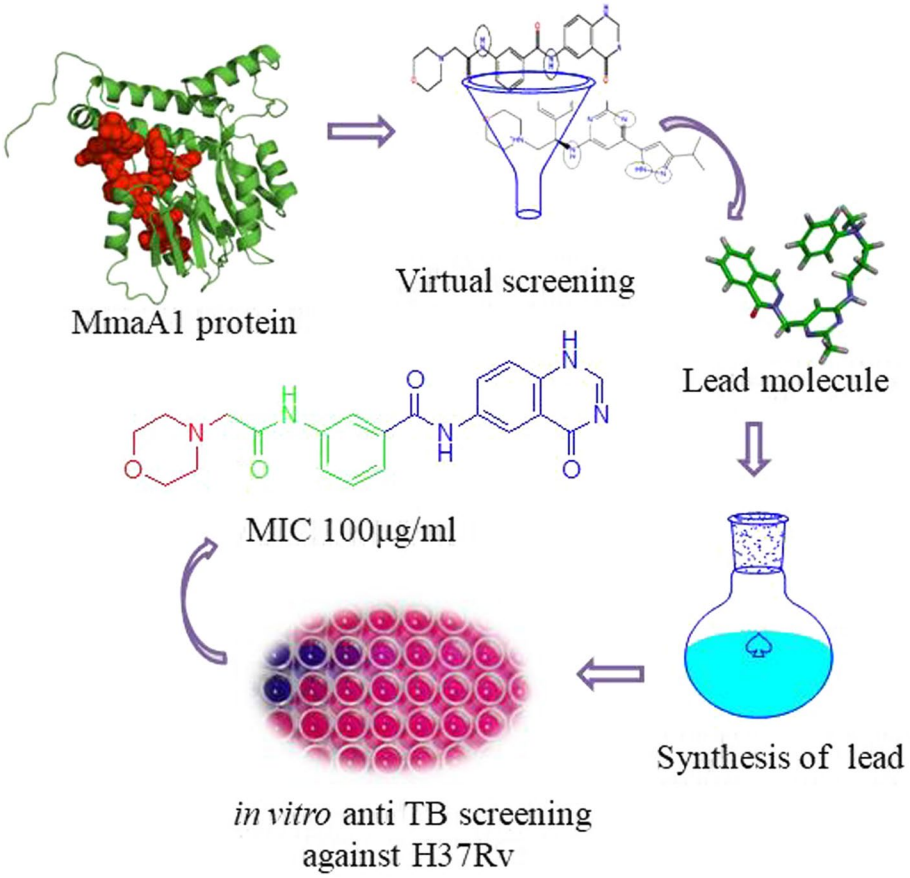

Keywords Tuberculosis · Mycolic acid methyl transferase · MmaA1 · Homology modelling · Virtual screening · MABA assay

Introduction

Tuberculosis (TB) is an air-borne infectious disease caused by the bacteria *Mycobacterium tuberculosis,* one of the top 10 leading causes of mortality across the globe. According to WHO global TB report 2019, it is estimated that 10 million people were affected and 1.2 million died due to this dreadful disease [1]. The main course of treatment for TB is the directly observed treatment, short-course (DOTS) therapy [2]. Currently, there are many new drugs in the discovery pipeline and some of them have been approved for the treatment like Bedaquiline (2012), Delamanid (2013) and Pretomanid (2019) [3–5]. The main drawbacks with TB treatment are resistance, long duration of treatment and drug toxicity. Therefore, this supports the search for new drug [6–8].

Mycolic acid methyl transferase (MmaA1)

Mycobacterium tuberculosis, the causative agent of the dreadful disease tuberculosis, has an intricate and complex cell wall structure. The complex, lipid-rich cell envelope is largely responsible for resistance and virulence of the *mycobacterium* which also acts as a permeability barrier. The cell wall of the *mycobacterium* is comprised of peptidoglycans, arabinogalactans and mycolic acids which are covalently bonded [9, 10]. Mycolic acids are long-chain α-alkyl β-hydroxy fatty acids, classified into alpha, methoxy and keto-mycolic acids [11, 12]. They are synthesised by two discrete elongation systems in *mycobacteria*, type I and type II fatty acid synthases (FAS I and FAS II, respectively) [13]. The synthesis of mycolic acids is followed by extensive post-synthetic modifications and unsaturations. These

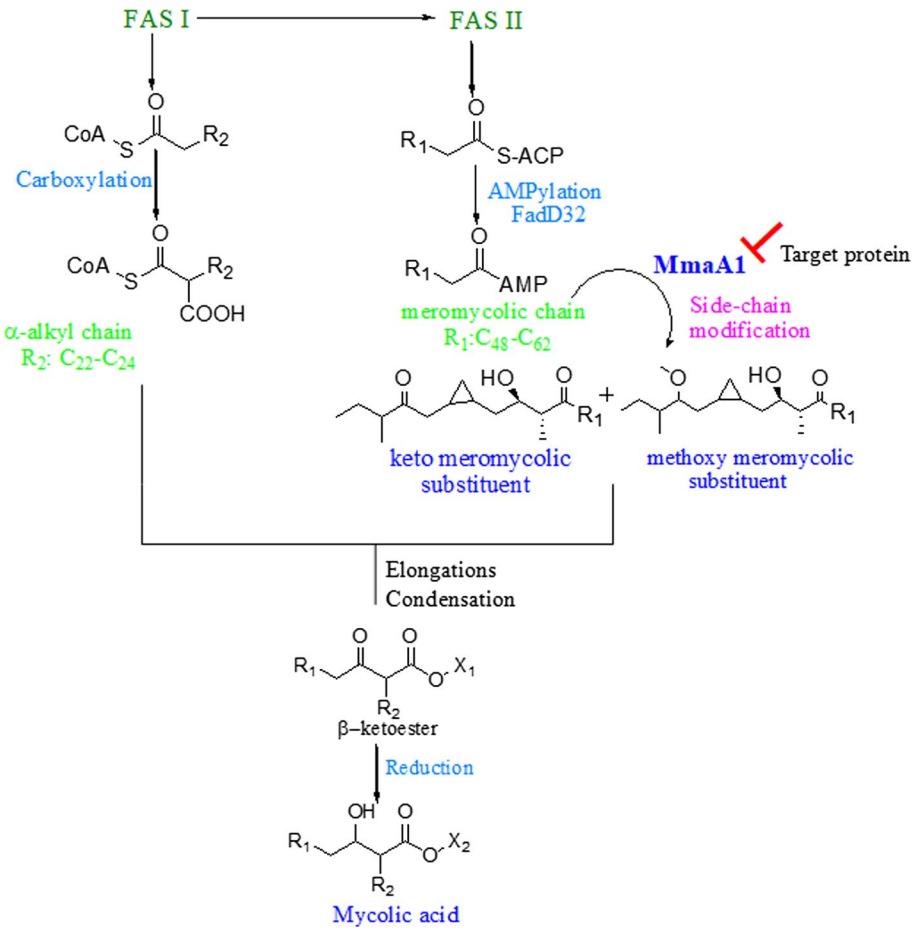

Fig. 1 Biochemical pathway of MmaA1 protein showing the role of MmaA1 protein in the biosynthesis of mycolic acids

post-synthetic modifications are brought about by a family of *S*-adenosyl-L-methionine (SAM)-dependent enzymes, which use meromycolic acid as a substrate to generate cis- and trans-cyclopropanes and other mycolic acids [14]. Mycolic acid methyl transferases belong to the mycolic acid cyclopropane synthases family, which play an important role in the synthesis of methoxy mycolic acids and have been designated as MmaA1–4 to indicate their involvement in the methoxy mycolic acid biosynthesis [15].

MmaA1 protein is essential for the synthesis of trans- and keto-mycolic acids in the mycobacterium, shown in Fig. 1. The MmaA1 protein converts cis-olefin oxygenated mycolate precursor to a trans-olefin with an adjacent methyl branch, i.e. to a trans-mycolic acid. Increase in trans-mycolic acid leads to increased cell wall rigidity, increased drug resistance and altered colony morphology [16]. Therefore, MmaA1 also acts as a branch point in the synthesis of trans- and keto-mycolic acids. Thus, inhibiting MmaA1 protein leads to inhibition of synthesis of mycolic acids resulting in loss of cell wall rigidity and ultimately cell death. Therefore, targeting MmaA1 protein can result in potential drug candidates for TB treatment [17, 18].

There is no reported 3-D structure for MmaA1 protein available in the protein data bank, and hence, we initiated homology modelling to facilitate the virtual screening study.

Materials and methods

Software

Webservers used for Active site prediction: CASTp, PatchDock.

Active site prediction: SiteMap, Schrodinger, LLC, New York, NY, 2010.

Docking: Glide, version 5.6, Schrodinger, LLC, New York, NY, 2010.

Docking analysis: Accelrys Discovery Studio, Schrodinger Suite.

ADMET studies: QikProp, version 3.4, Schrodinger, LLC, New York, NY, 2011.

Homology modelling of MmaA1 protein

The FASTA sequence of the protein was retrieved from the ExPASy Proteomic server (Uniprot ID: P9WPB1) [19]. The sequence was then screened for similarity search against all the proteins deposited in Protein Data Bank [20] using template and similarity search programs such as Basic Local Alignment Search Tool (BLASTp) [21] and JPred3 server [22]. The alignment of identified template and target proteins was executed using ClustalW [23]. The 3-D model of the protein was generated using MODELLER 9v13 [24].

Model validation

The obtained 3-D model of the protein was evaluated using PROCHECK [25] and Verify_3D [26] available from the Structural Analysis and Verification Server (SAVES) and ProSA server [27]. The PROCHECK server analyses the stereochemical quality of the protein and gives an assessment of overall quality of the structure compared to well-refined structures of similar resolution, which is given by the Ramachandran (RC) plot [28, 29].

The accuracy of a protein 3-D structure can be determined by Verify_3D, which tests the quality of protein structures by comparing them with the 3-D profiles of correct protein structures having high scores. ProSA is a widely used tool to check potential errors in 3-D models of proteins which are obtained either from experimental elucidation, from protein engineering or theoretical models. The program gives a *z*-score plot and energy plot for the protein. The energy of the structure is evaluated using a distance-based and solvent exposure potential of protein residues. The *z*-score is indicative of overall model quality of the protein 3-D structure. The ProSA energy plot determines the local quality of the 3-D model by plotting energy as a function of amino acid sequence position. Positive values correspond to erroneous parts, whereas negative values indicate a stable and good model.

Active site prediction

The binding of the ligand in the active site of the protein is brought about by the microenvironment, which is created by folds of the 3-D structure of protein into cavities or pockets. The knowledge of structure of the cavities of proteins helps in designing novel ligands, enzyme inhibitors, understanding their binding modes and protein dynamics. In the present study, active site of the protein was identified using CASTp

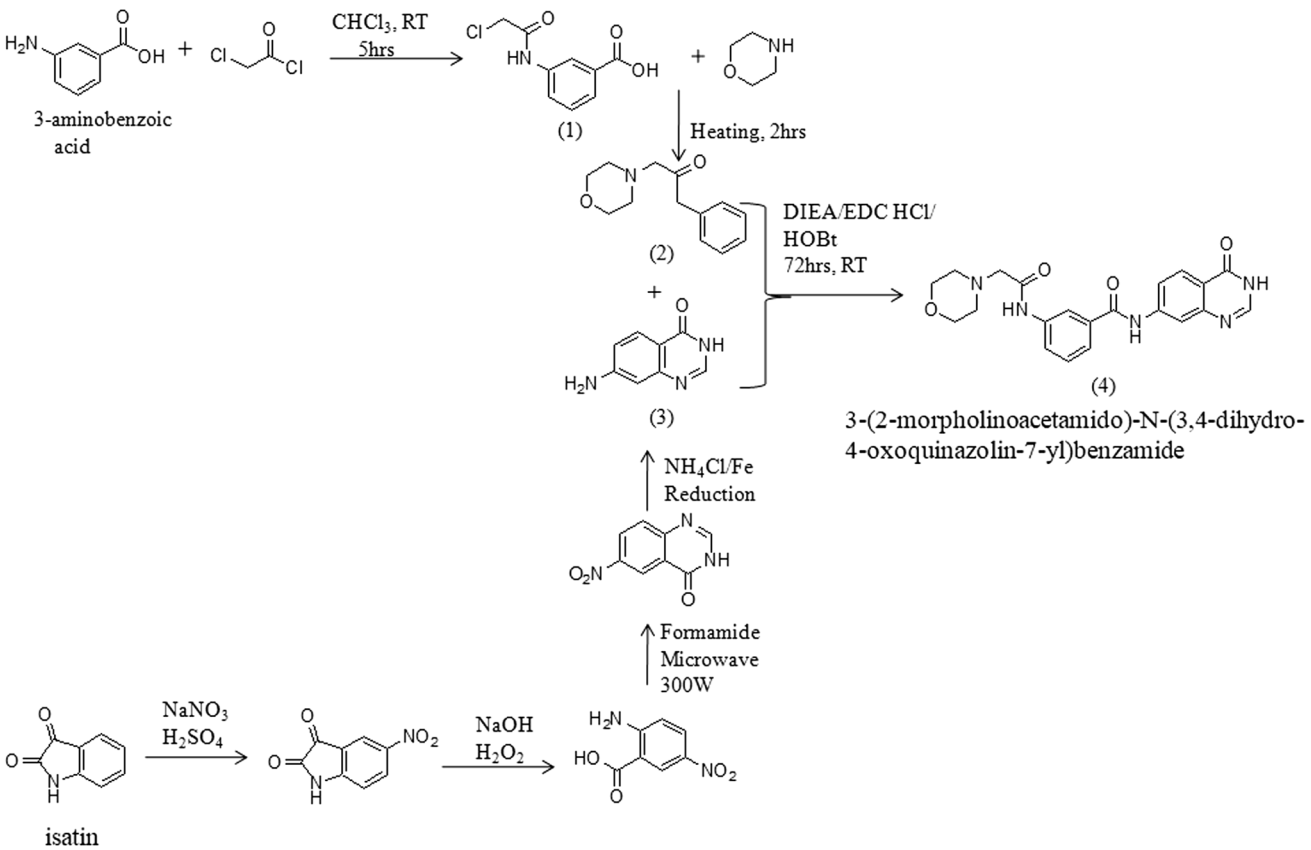

Scheme 1 Synthesis scheme of 3-(2-morpholinoacetamido)-*N*-(3, 4-dihydro-4-oxoquinazolin-7-yl)benzamide

(Computed Atlas of Surface Topography of proteins) server [30], SiteMap [31] and PatchDock online webserver [32]. PatchDock was used to carry out protein–ligand docking of the MmaA1 protein with its natural substrate *S*-adenosyl-*N*-decyl-aminoethyl (SADAE) [33]. A grid was generated by the Receptor grid generation module of Glide taking into consideration the predicted active site residues.

Virtual screening

Virtual screening is a fast and cost-effective tool for screening of compound databases in search of novel lead molecules. This method can be used for screening large libraries of chemicals for compounds that complement targets of known structure [34]. Computational screening or docking methods are improving at an incredible rate providing newer versions which have become complementary alternatives to high-throughput screening [35]. In the present work, Grid-based Ligand Docking with Energetics (Glide) module of Schrodinger Suite [36] was used for docking. The virtual screening process is carried out in four stages in Glide, namely protein preparation, ligand preparation, grid generation and virtual screening.

The MmaA1 protein was prepared for docking by submitting it to the Protein preparation wizard module of Schrodinger Suite. OPLS-2005 force field was used for allocation of bond orders [37]. This step is followed by energy minimisation using Impref module of Schrodinger Suite, using OPLS-2005 force field, with a cutoff RMSD of 0.3 Å between successive conformations, in the minimisation process [38].

The 3-D coordinates of the ligands were optimised using LigPrep module of Schrodinger Suite [39]. The stereoisomers with specific chiralities were retained to generate five conformers per ligand. The pre-filtering process also includes elimination of reactive functional groups and to improve the pharmacokinetic properties of the ligands for further study. The Receptor Grid generation module in Protein preparation wizard was used for grid generation.

In the virtual screening stage, the ligand molecules are docked at the predicted active site of the protein using Glide module of Schrodinger suite. Glide uses a series of modules which act as hierarchical filters, namely high-throughput virtual screening, standard precision (sp) and extra precision (XP) to minimise false positives and false negatives from entering into final phases of docking results [40]. The glide score and glide energy were used for prioritising the ligand molecules.

In silico ADME prediction

The absorption, distribution, metabolism and elimination are crucial properties for the clinical success of a drug candidate. Nearly 50% of the drugs fail because of poor ADME properties [41, 42]. Advances have been made in the in silico prediction of ADME properties of molecules, which resulted in a number of programs available for predicting several parameters/descriptors for this purpose. Predicting ADME reduces animal testing, reduces cost and time and provides reliable toxicity prediction. In the present study, the ADME properties were predicted using QikProp [43].

Experimental

All the solvents and chemicals were purchased from commercial sources and used without further purification. The reactions were monitored on pre-coated silica gel TLC using appropriate mobile phase. Visualisation of the spots was done with the help of UV at 254 nm. Biotage Initiator system was used for microwave reactions. For column chromatography, stationary phase: silica gel, mobile phase: chloroform–methanol, gradient elution method was used. Melting points were noted by using DigiMelt (Stanford Research Systems, USA) and are uncorrected. IR spectral data were recorded on Bruker ALPHA-T FTIR system using KBr pellet method. ^{1}H and ^{13}C NMR spectra were recorded on Bruker (400 MHz for ^{1}H and 100 MHz for ^{13}C) instrument. $CDCl_3$ and DMSO-d_6 were used as NMR solvents and tetramethylsilane (TMS) as an internal standard. Chemical shifts (δ) values were referenced to the residual solvent peak and reported in ppm, and all coupling constant (J) values were given in Hz. The following multiplicity abbreviations are used: (s) singlet, (d) doublet, (t) triplet, (m) multiplet, (q) quartet, (dd) double doublet. HRMS data were measured on Agilent 6530 Q-TOF LC-HRMS system, ESI method, positive mode. The instrument was tuned using an Agilent tune mix. A reference solution (m/z 121.0509, m/z 922.0098) was used to correct small mass drifts during the acquisition. Analyses indicated by the symbols of the elements or functions were within ± 0.4% of theoretical values.

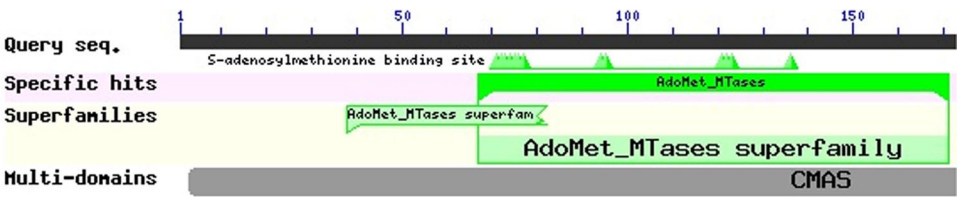

Fig. 2 Conserved domains of MmaA1 protein

Table 1 Template search results for MmaA1 protein

S. no.	Name of the server	Parameters considered for template selection	*E* value	PDB code of template protein
1	BLAST	Sequence position specificity	4e−116	1KP9_A
2	JPred3	Secondary structure prediction, solvent accessibility and coiled-coil region prediction	1e−89	1KP9_A

The servers predicted 1KP9_A as template for the MmaA1 protein

Synthesis of 3-(2-morpholinoacetamido)-*N*-(3,4-dihydro-4-oxoquinazolin-7-yl) benzamide

All the top 10 compounds obtained from virtual screening study were analysed for novelty and synthetic feasibility based on literature search and SciFinder search studies. The compound 3-(2-morpholinoacetamido)-*N*-(3,4-dihydro-4-oxoquinazolin-7-yl) benzamide was selected for synthesis based on this analysis. The scheme of synthesis for the title compound is given in Scheme 1. The starting materials for synthesis in this scheme are 3-aminobenzoic acid and isatin. The compound (1), 3-(2-chloroacetamido) benzoic acid was synthesised from 3-aminobenzoic acid (0.4 mmol) and chloroacetyl chloride (0.5 mmol) in dry benzene at RT by stirring for 5 h [44]. After completion of the reaction as indicated by TLC, the reaction mixture was poured onto crushed ice, stirred, filtered and dried under vacuum to obtain a white colour solid, which was further re-crystallised from chloroform/methanol (9:1) mixture. The compound (2), 3-(2-morpholinoacetamido) benzoic acid was obtained by treating compound (1) (2.34 mmol) and morpholine (5.68 mmol) with ethyl acetate as solvent and heating at 80 °C for 2 h. A brown colour gummy solid was obtained which was separated and purified using chromatographic column (dry packing method), silica gel as stationary phase and chloroform–methanol mobile phase eluted by gradient method.

The synthesis of compound (3) was brought by a series of reactions using isatin as the starting material. Isatin (0.068 mmol) was dissolved in 12 ml sulphuric acid at 0 °C. To this sodium nitrate (0.068 mmol) dissolved in sulphuric acid was added dropwise and kept for stirring for 4 h at 0 °C [45]. The reaction mixture was poured onto crushed ice, filtered and dried to obtain a yellow colour solid, 5-nitro isatin. The 5-nitro isatin (0.99 mmol) was subjected to oxidation at RT for 15 min using 5% sodium hydroxide solution and hydrogen peroxide (0.032 mmol). Then, dil. HCl was added and pH adjusted to 1 to obtain 5-nitro anthranilic acid [46]. It was then filtered and dried to obtain a pale yellow solid.

To 5-nitro anthranilic acid (5 mmol) and formamide (50 mmol), catalytic amount of acetic acid was added and kept in microwave oven for 10 min at 300 W [47]. The reaction mixture was quenched on ice and filtered to obtain a brown colour solid, 7-nitroquinazolin-4(3H)-one. To 7-nitroquinazolin-4(3H)-one (2.61 mmol), in ethanol as solvent, ammonium chloride (26.16 mmol) dissolved in water and iron powder (10.39 mmol) were added and kept for reflux for 4 h to obtain the compound (3), 7-aminoquinazolin-4(3H)-one. The reaction mixture was filtered under vacuum. The filtrate was evaporated under vacuum to obtain a grey colour solid which was further re-crystallised using methanol/charcoal to obtain grey coloured shiny needle shape crystals.

The synthesis of the title compound (4), 3-(2-morpholinoacetamido)-*N*-(3,4-dihydro-4-oxoquina-

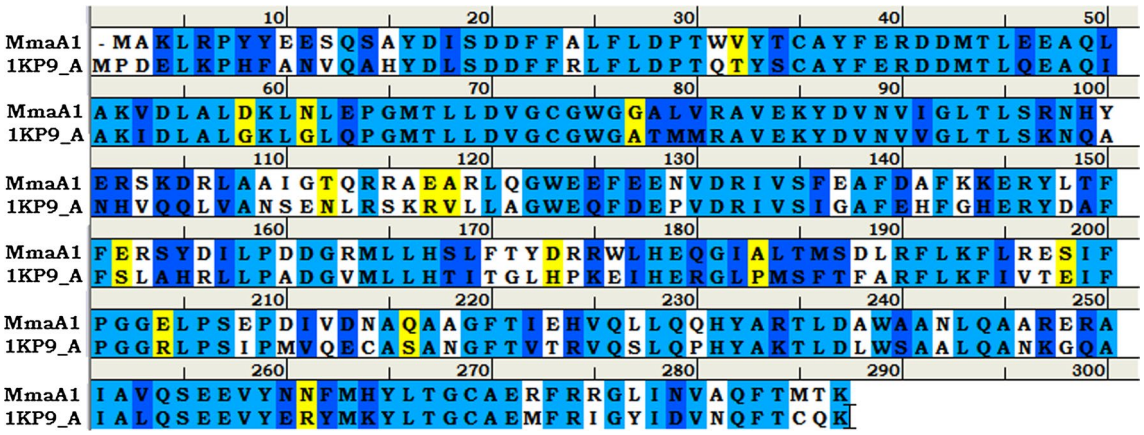

Fig. 3 Sequence alignment of MmaA1 protein with the template (1KP9_A) showing identical residues in blue colour, strongly similar residues in dark blue colour and weakly similar residues in yellow colour

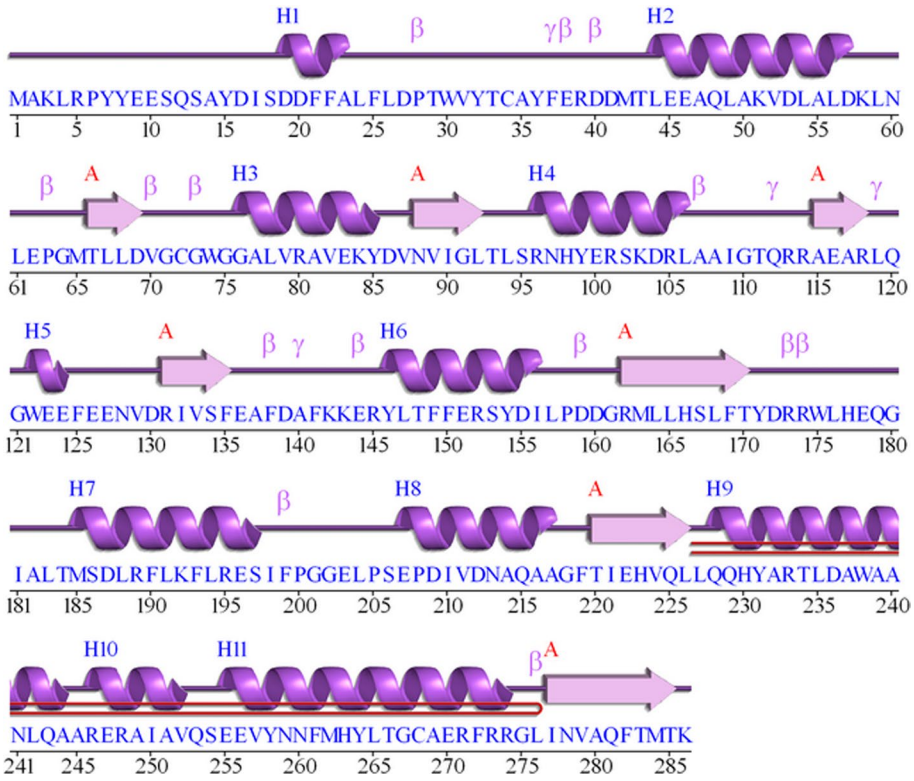

Fig. 4 The secondary structure of MmaA1 protein shown in purple colour helices and sheets predicted by PDBsum. The red line represents β-hairpin motif

Table 2 Details of secondary structure of the MmaA1 protein showing α-helices

S. no.	Start of α-helix	End of α-helix	No. of residues	Sequence
1	ASP19	ALA23	5	DDFFA
2	LEU44	ASP57	14	LEEAQLAKVDLALD
3	GLY76	TYR85	10	GALVRAVEKY
4	ARG96	ALA106	11	RNHYERSKDRL
5	TYR146	ILE156	11	YLTFFERSYDI
6	MET185	SER197	13	MSDLRFLKFLRES
7	GLU207	ALA217	11	EPDIVDNAQAA
8	GLU228	ALA244	17	QQHYARTLDAWAANLQA
9	ARG246	VAL252	7	RERAIAV
10	GLU255	ARG274	20	EEVYNNFMHYLTGCAERFRR

The secondary structure of MmaA1 protein has 10 α-helices predicted using ProFunc of PDBsum

zolin-7-yl) benzamide was brought about by acid amide coupling [48]. To 3-(2-morpholinoacetamido) benzoic acid, (1.403 mmol, 1 eq), DIEA (1.665 mmol, 2.5 eq) was added under ice cold conditions and kept for stirring for 5 min, then EDC HCl (1.987 mmol, 1.2 eq), HOBt (2.383 mmol, 1.2 eq) and 7-aminoquinazolin-4(3H)-one (2.383 mmol, 0.26 eq) were added and kept for stirring at RT for 72 h. The solvent was evaporated under vacuum, and re-crystallised with hexane–ethyl acetate (1:2) to obtain a highly hygroscopic brown colour solid.

In vitro anti-TB activity study of 3-(2-morpholinoacetamido)-*N*-(3,4-dihydro-4-oxoquinazolin-5-yl)benzamide and its intermediates

Microplate Alamar Blue Assay (MABA) is a rapid, high-throughput, inexpensive dye-based cell viability assay which uses Alamar blue as indicator for anti-mycobacterial drug screening. MABA helps in quantitative determination of drug susceptibility of replicating *M. tuberculosis* [49, 50]. The

Table 3 Details of the secondary structure of the MmaA1 protein showing β-sheets

S. no.	Start of β-sheet	End of β-sheet	No. of residues	Sequence
1	THR66	VAL70	5	TLLDV
2	ASN88	LEU92	5	NVIGL
3	ALA115	ARG118	4	AEAR
4	ARG131	PHE135	5	RIVSF
5	ARG162	THR170	9	RMLLHSLFT
6	THR220	LEU226	7	TIEHVQL
7	ILE277	THR285	9	INVAQFTMT

The secondary structure of the MmaA1 protein has 7 β-sheets predicted using ProFunc of PDBsum

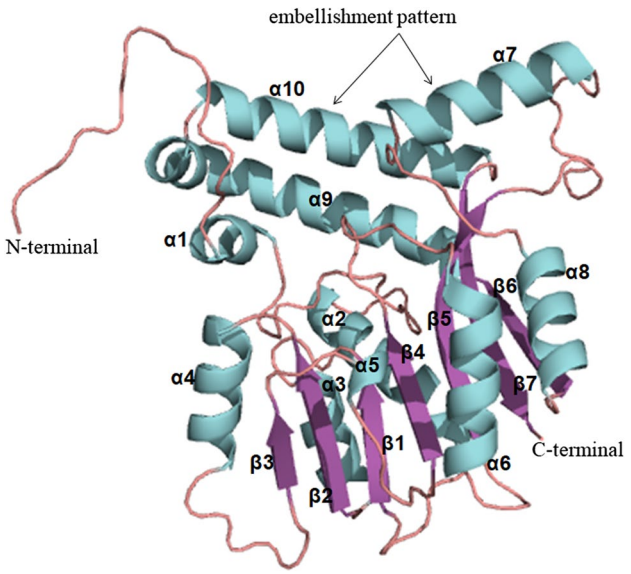

Fig. 5 3-D model of MmaA1 protein

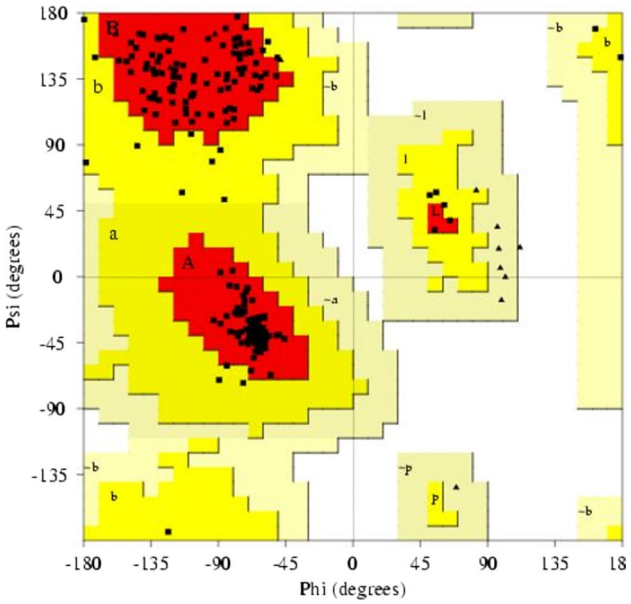

Fig. 6 Ramachandran plot of MmaA1 protein

Table 4 Ramachandran plot statistics of MmaA1 protein

Description	No. of amino acids	Percentage
Residues in most favoured regions	243	92.7%
Residues in additional allowed regions	19	7.3%
Residues in generously allowed regions	0	0.0%
Residues in disallowed regions	0	0.0%
Number of non-glycine and non-proline residues	262	100.0%
Number of end-residues (excl. Gly and Pro)	2	
Number of glycine residues (shown as triangles)	15	
Number of proline residues	7	
Total number of residues	286	

synthesised compound 3-(2-morpholinoacetamido)-*N*-(3,4-dihydro-4-oxoquinazolin-5-yl)benzamide and its intermediates were evaluated for their in vitro anti-tubercular activity against H37Rv strain using the Microplate Alamar Blue susceptibility test, and the activity is given as minimum inhibitory concentration (MIC) in µg/ml.

Results and discussion

Structural evaluation of MmaA1 protein

The FASTA sequence of MmaA1 protein (Accession no. P9WPB1) was obtained from Expasy Proteomics tool (Uniprot) from Server Expert Protein Analysis System (Expasy SWISS-PROT/TrEMBL) database. The conserved domains of the protein predicted using BLAST server are shown in Fig. 2. The predicted domain *S*-adenosyl methionine binding site extends from ASP 70–LEU 170. The template search result from BLAST predicted the Apo-form of Mycolic acid cyclopropane synthase (Cmaa1), PDB code: 1KP9_A to have the highest identity of 57% and *E* value of 4e−116 and JPred3 server predicted an *E* value of 1e−89 for the protein 1KP9_A. The *E* values with the corresponding templates are given in Table 1.

The MmaA1 protein sequence alignment with the template protein 1KP9_A shows a 76% sequence similarity shown in Fig. 3. Therefore, the protein Mycolic acid cyclopropane synthase (Cmaa1) was taken as the template for model generation based on the sequence alignment and

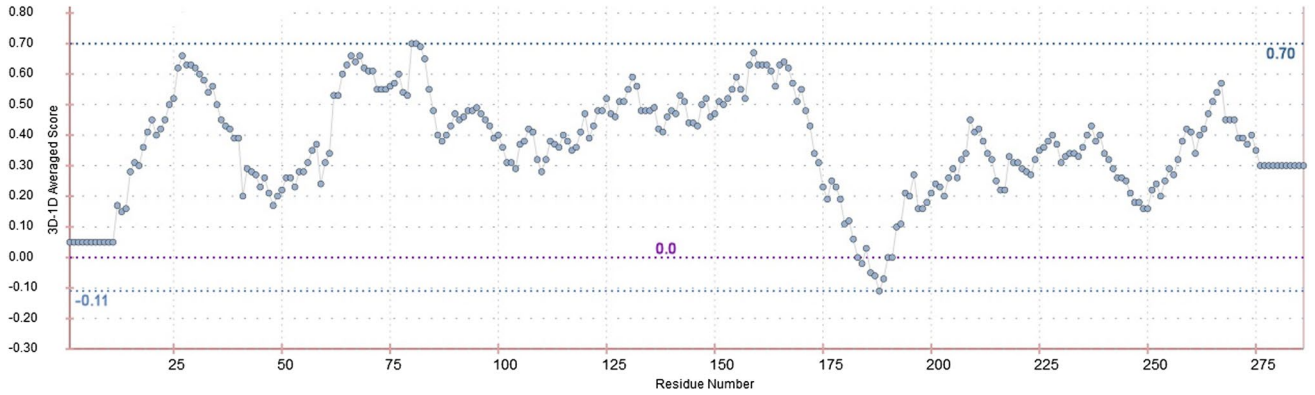

Fig. 7 Verify_3D plot of MmaA1 protein

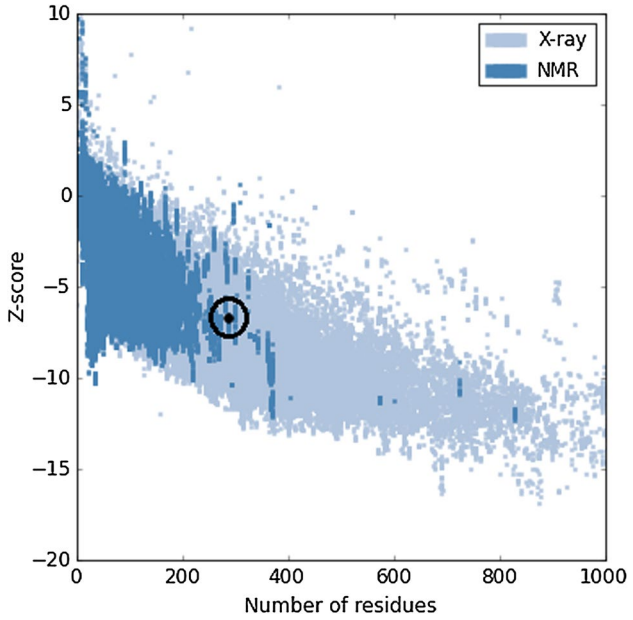

Fig. 8 z-plot of MmaA1 protein obtained ProSA webserver. The black spot encircled corresponds to MmaA1 protein

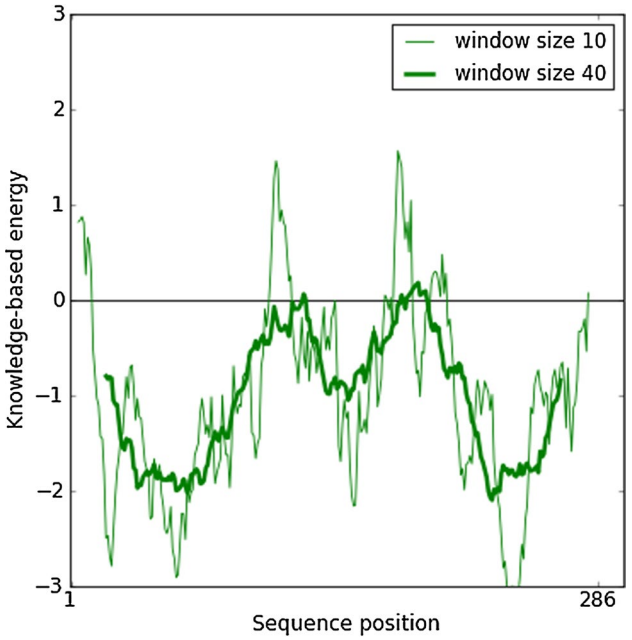

Fig. 9 ProSA energy plot of MmaA1 protein

predicted *E* values. The secondary structure of MmaA1 protein is shown in Fig. 4 which consists of ten α-helices and seven β-sheets. The residues corresponding to the secondary structure which are predicted using ProFunc (Prediction of protein function from 3-D structure) [51] of PDBsum webserver are given in Tables 2 and 3.

The α-helices in the secondary structure of MmaA1 protein form an embellishment pattern shown in Fig. 5 which is characteristic of Mycolic acid *S*-adenosyl methyl transferases (SAM-MTs). The protein core consists of seven β-strands parallel to each other except β-strand 7, flanked on each side by three helices. There is a β-hairpin motif between the seven residues in β strand 6 (THR 220–LEU 226) to the nine residues in β-strand 7 (ILE 277–THR 285). β-hairpins consist of two β-strands which are anti-parallel and are hydrogen bonded together.

Model refinement and validation

The Ramachandran plot of MmaA1 protein is shown in Fig. 6 obtained from SAVES server. The plot statistics are given in Table 4. The plot statistics show that 92.7% of amino acid residues are in most favoured region, 7.3% in additionally allowed region and none of the residues in the generously allowed or disallowed regions. Therefore, the

Table 5 Active site regions predicted for MmaA1 protein

S. no.	Server	Active site residues
1	CASTp	TYR32-CYS34, ASP69-ARG80, LEU92-ARG101, GLN120-GLU123, SER134-ALA140
2	SiteMap	SER13-PHE22, TRP30, TYR32, GLU46, ASP69-ALA81, LEU92-LEU 94, HIS98, TRP122, SER134-TYR146, LEU165, ASN260-TYR264
3	PatchDock	TYR 32, THR 33, TRP 74

generated 3-D model is a good-quality model in terms of stereochemical quality.

The Verify_3D plot of MmaA1 protein is shown in Fig. 7. The plot shows that 86.7% of the residues have an averaged 3D-1D score ≥ 0.2. A good-quality structure requires at least 80% of the amino acids to have a score ≥ 0.2 in the 3D/1D profile.

The MmaA1 protein was submitted to ProSA webserver, and a *z*-score of − 6.69 was obtained. The plot shows *z*-scores of all protein chains in PDB determined by X-ray crystallography (light blue colour region) and by NMR spectroscopy (dark blue region) shown in Fig. 8.

Figure 9 shows the energy profile of MmaA1 protein obtained using ProSA web server. The obtained ProSA energy plot for the model shows maximum residues within negative region of energy, which indicate that the MmaA1 model is a stable model.

Active site identification

The binding site predictions for MmaA1 protein from CASTp, SiteMap and protein ligand docking are given in Table 5. Figure 10 depicts the active site of MmaA1 protein generated using PyMOL [52]. The MmaA1 protein predicted active site extends in the residue domain ranging from SER13–PHE22, TRP30, TYR32–CYS34, GLU46, ASP69–ALA81, LEU92–ARG101, GLN120–GLU123, SER134–TYR146, LEU165, ASN 260–TYR264. The active site of MmaA1 protein was generated and considered for grid generation in virtual screening using these predicted residues.

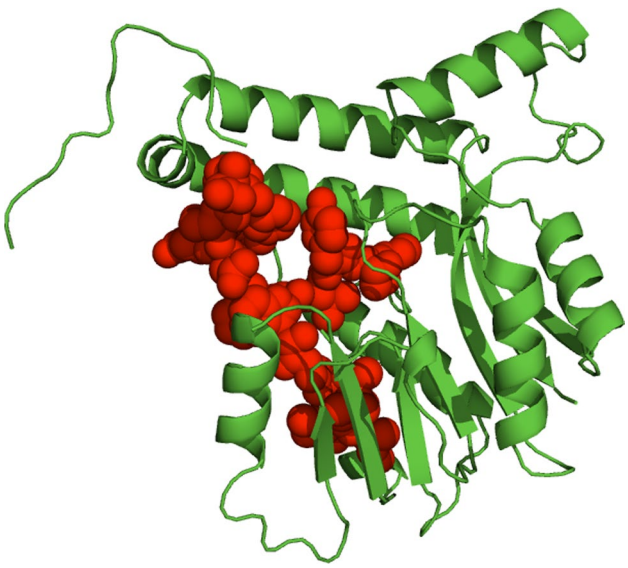

Fig. 10 Active site of MmaA1 protein. The protein is represented as green colour ribbon model, and active site residues are represented as red colour spheres

Virtual screening

In the present study, structure-based virtual screening was carried out for MmaA1 protein using two small molecule ligand databases: Asinex synergy and Diverse_Elite_Gold_Platinum using protocols reported earlier [53, 54]. Asinex synergy database consisting of 36,411 compounds was subjected to ligand preparation. The stereoisomers with specific chiralities were retained to generate five conformers per ligand. The stable conformers were retained, and an output of 1,17,159 stereoisomeric structures were generated. The generated conformers were subjected to HTVS mode to obtain an output of 12,896 structures. These output structures were further screened successively in SP and XP modes with a filtration ratio of 10% at each stage of docking as reported earlier [55]. This screening process gave an output of 128 structures of docked complexes. The criteria for filtration of ligands at each stage include good docking and scoring poses.

The protocol followed for Asinex synergy database was applied to the virtual screening of Diverse_Elite_Gold_Platinum database as well. The Diverse_Elite_Gold_Platinum database consists of 7035 molecules and after subjecting to ligand preparation gave an output of 13,655 conformers and further virtual screening process through HTVS, SP and XP modes gave an output of 13 docked complexes. All these complexes can be considered for the identification of potent ligands as inhibitors for MmaA1 protein. A total of 141 docked complexes were obtained from virtual screening process with Glide scores ranging from − 13 to − 12. The resulting docked complexes were visually inspected, analysed and prioritised based on Glide score. A sample of top 10 molecules (M1–M10) are given in Table 6 prioritised based on Glide docking score. The

Table 6 Ligands showing Glide score and Glide energy with intermolecular interactions and bond distance in Angstroms

S. no.	Structure	Glide score	Glide energy	Intermolecular interactions	Bond distance (Å)
1	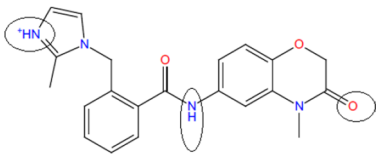	− 13.4	− 53.5	*Hydrogen bonds*	
	2-methyl-1-(2-(4-methyl-3-oxo-3,4-dihydro-2H-benzo[b][1, 4]oxazin-6-yl carbamoyl)benzyl)-1H-imidazol-3-ium			ALA77:H-M1:O19	2.038
				M1:H28-TRP30:O	2.126
				Pi–Pi interactions	
				TYR32-M1:N48	4.695
				PHE22-M1:N48	4.715
2	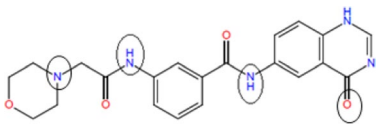	− 12.7	− 65.20	*Hydrogen bonds*	
	3-(2-morpholinoacetamido)-*N*-(3,4-dihydro-4-oxoquinazolin-7-yl) benzamide			TRP74:HE1-M2:N2	1.950
				GLY76:M2:N-O16	2.386
				M2:H29-TRP30:O	1.804
				M2:H34-ASP19:OD1	2.271
				M2:H52-ASP19:OD1	2.088
				Pi–Pi interactions	
				PHE22-M2:N55	4.924
				M2:NZ-LYS51	6.752
3	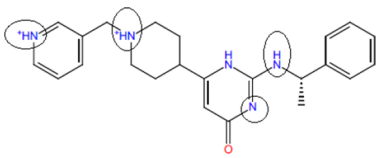	− 12.4	− 56.17	*Hydrogen bonds*	
	(S)-3-((4-6-oxo-2-(1-phenyl ethylamino)-3,6-dihydropyrimidin-4-yl)piperidinyl) methyl)pyridinium			TRP74:HE1-M3:N2	1.950
				M3:H29-TRP30:O	2.386
				M3:H58-ASP16:OD1	1.804
				Pi–Pi interactions	
				PHE22-M3:N55	4.924
4	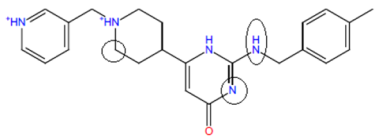	− 12.4	− 51.1	*Hydrogen bonds*	
	3-((4-(2-(4-methylbenzylamino)-6-oxo-3,6-dihydropyrimidin-4-yl)piperidinium-1-yl)methyl) pyridinium			TRP74:HE1-M4:N1	1.800
				M4:H29-TRP30:O	2.142
				Pi–Pi interactions	
				PHE22-M4:N55	5.804
5	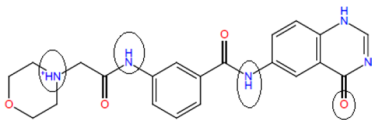	− 12.2	− 61.9	*Hydrogen bonds*	
	4-(2-oxo-2-(3-(4-oxo-1,4-dihydro quinazolin-6-yl carbamoyl) phenyl amino)ethyl) morpholin-4-ium			M5:H33-TRP30:O	2.094
				M5:H35-ASP19:OD1	1.939
				Pi–Pi interactions	
				M5-LYS51:NZ	6.050
				M5-LYS51:NZ	6.966

Table 6 (continued)

S. no.	Structure	Glide score	Glide energy	Intermolecular interactions	Bond distance (Å)
6	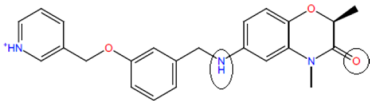	− 11.8	− 45.6	*Hydrogen bonds*	
	(S)-3-((3-((2,4-dimethyl-3-oxo-3,4-dihydro-2H-benzo[b][1, 4]oxazin-6-ylamino) methyl)phenoxy)methyl)pyridinium			ALA77:H-M6:O8	1.946
				M6:H32-TRP30: O	1.884
				Pi–Pi interactions	
				PHE22-M6	4.047
				TYR32-M6:N52	6.520
7	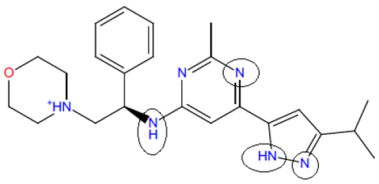	− 11.6	− 49.0	*Hydrogen bonds*	
	(R)-4-(2-(6-(3-isopropyl-1H-pyrazol-5-yl)-2-methylpyrimidin -4-ylamino)-2-phenylethyl) morpholin-4-ium			TYR32:H-M7:N9	2.484
				TRP74:HE1-M7:N2	2.001
				M7:H31-TRP30:O	1.636
				M7:H33-GLY71:O	2.266
8	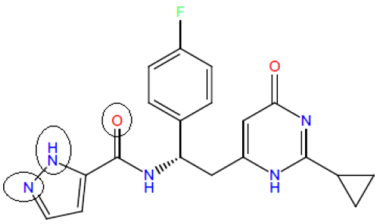	− 11.3	− 54.4	*Hydrogen bonds*	
	(S)-N-(2-(2-cyclopropyl-6-oxo-3,6-dihydropyrimidin-4-yl)-1-(4-fluorophenyl) ethyl)-1H-pyrazole-5-carboxamide			TYR32:H-M8:O20	1.907
				TRP74:HE1-M8:N15	2.025
				M8:H36-TRP30:O	1.687
				Pi–Pi interactions	
				M8-PHE135	5.463
9	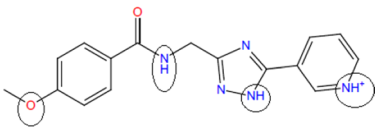	− 11.3	− 47.8	*Hydrogen bonds*	
	3-(3-((4-methoxybenzamido)methyl)-1H-1,2,4-triazol-5-yl)pyridinium			ALA77:H-M9:O18	2.323
				M9:H23-TRP30:O	2.058
				M9:H24-GLY71:O	2.255
				Pi–Pi interactions	
				M9-VAL31:HG22	2.907
				PHE22-M9:N38	4.316
				TYR32-M9:N38	5.511
10	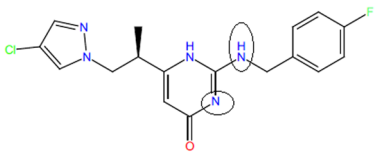	− 11.3	− 49.4	*Hydrogen bonds*	
	(R)-2-(1-(4-chloro-1H-pyrazol-1-yl)propan-2-yl)-6-(4-fluoro benzyl amino) pyridine-4(1H)-one			TRP74:HE1-M10:N1	2.913
				M10:H32-TRP30:O	2.195
				Pi–Pi interactions	
				PHE22-M10	4.776

Ligand structures and intermolecular interactions between the protein MmaA1 and the ligands of the docked complexes. The functional groups forming hydrogen bonds and pi–pi interactions have been highlighted in circles

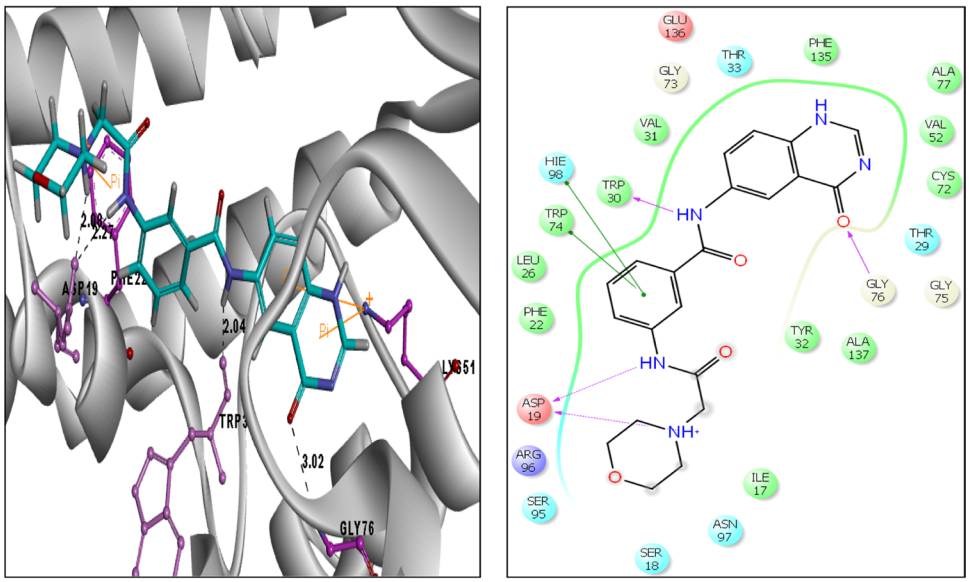

Fig. 11 **a** Binding interaction of 3-(2-morpholinoacetamido)-*N*-(3,4-dihydro-4-oxoquinazolin-7-yl) benzamide with MmaA1 protein, **b** 2-D view of binding interaction of 3-(2-morpholinoacetamido)-*N*-(3,4-dihydro-4-oxoquinazolin-7-yl) benzamide with MmaA1 protein

Table 7 Predicted ADME or pharmacokinetic values of the top ten docked molecules for MmaA1 protein

S.no.	Mol.wt.	CNS	Donor HB	Accept HB	Rule of five	Rule of three	QPlogPo/w	QPlog BB	QPlog HERG	%Human oral absorption
M1	436	1	1.0	5.75	1	2	5.06	−0.29	−6.69	100
M2	407	−2	3.0	12.2	0	0	0.47	−1.36	−7.16	58
M3	389	1	2.0	7.5	0	0	3.26	−0.64	−7.43	86
M4	389	0	2.0	7.5	0	0	2.96	−0.75	−7.12	82
M5	407	−2	3.0	12.2	0	0	0.39	−1.34	−7.08	57
M6	389	0	1.0	7.0	0	1	4.11	−0.53	−6.51	100
M7	406	1	2.0	7.2	0	0	3.58	−0.31	−6.42	93
M8	367	−2	3.0	7.0	0	0	2.56	−1.35	−5.46	83
M9	309	−1	2.0	7.25	0	0	1.76	−0.93	−5.87	87
M10	361	0	2.0	5.5	0	0	3.87	−0.59	−5.90	100

binding pose, hydrogen bond and pi–pi interaction of the synthesised ligand, 3-(2-morpholinoacetamido)-*N*-(3,4-dihydro-4-oxoquinazolin-7-yl) benzamide with MmaA1 protein from docked complex is shown in Fig. 11a and b. The protein ligand interactions were visualised using Accelrys Discovery Visualiser [56].

ADME analysis

The evaluation of ADME properties is an essential part of drug discovery to minimise failures of drug candidates in clinical phase. In the present study, the ADME properties were predicted using QikProp module of Schrodinger suite, given in Table 7. The physicochemical properties such as molecular weight and descriptor values of donor hydrogen bonds, acceptor hydrogen bonds are in acceptable range. All the top 10 ranking molecules obey Lipinski's rule of five, Jorgensen rule of three and various other important pharmacokinetic parameters. The molecules M1, M6 and M10 show 100% human oral absorption, and the molecules M3, M4, M7, M8 and M9 show more than 80% human oral absorption. The other important descriptors which are responsible for the drug candidate to be successful in the drug discovery are CNS activitiy, QPlogBB (predicted brain/blood partition coefficient) and QPlogHERG (predicted IC50 value for blockage of HERG K + channel) and are in permissible limits for the top 10 molecules in the present study. Therefore, the molecules

obtained from virtual screening in the present study have ADME properties within acceptable range which show that these molecules have good drug-like properties.

Characterisation of synthesised compounds

Compound (1): 3-(2-chloroacetamido) benzoic acid

White solid; Yield: 93%; mp: 220.6 °C; IR (KBr): 1593, 1675, 3088, 3272 cm^{-1}; ^{1}HNMR (400 MHz, DMSO-D_6): δ 4.27 (s, 2H), 7.48 (t, $J=8$, 1H), 7.68 (d, $J=7.6$ Hz, 1H), 7.82 (t, $J=8$, 1H), 8.23 (s, 1H), 10.51 (s, 1H); ^{13}CNMR (100 MHz, DMSO-D_6): δ 43.99, 120.54, 123.93, 125.10, 129.65, 131.88, 139.16, 165.38, 167.49; HRMS (ESI): *m/z* calcd. for $C_9H_8ClNO_3$ $[M+H]^+$: 214.02, found 214.0276; Anal calcd. for $C_9H_8ClNO_3$: C: 50.60; H: 3.77; N: 6.56%; found C: 50.58; H: 3.75; N: 6.55%; anti-TB activity MIC (H37Rv assay): 25 µg/ml.

Compound (2): 3-(2-morpholinoacetamido) benzoic acid

Pale brown solid; Yield: 90%; mp: 91.5 °C; IR (KBr): 1106, 1517, 1662, 2854, 2923 cm^{-1}; ^{1}HNMR (400 MHz, DMSO-D_6): 2.88 (s, 1H), 3.14 (s, 3H), 3.65 (t, $J=9.2$ Hz, 6H), 7.43 (t, $J=8$ Hz, 1H), 7.64 (d, $J=8$ Hz, 1H), 7.86 (d, $J=8$ Hz, 1H), 8.25 (s, 1H), 9.92 (s, 1H); ^{13}CNMR (100 MHz, DMSO-D_6):δ 169.61, 168.65, 138.63, 136.86, 128.55, 124.75, 122.29, 120.97, 66.55, 65.31, 62.47, 53.61, 44.07; HRMS (ESI): *m/z* calcd. for $C_{13}H_{16}N_2O_4$ $[M+H]^+$: 265.11, found: 265.1164; Anal calcd. for $C_{13}H_{16}N_2O_4$: C: 59.08; H: 6.10; N: 10.60%; found C: 59.06; H: 6.10; N: 10.58%; anti-TB activity MIC (H37Rv assay): 25 µg/ml.

Compound (3): 7-aminoquinazolin-4(3H)-one

Grey solid; Yield: 80%; mp: 232.90C; IR (KBr): 1676, 2908, 2951, 3170 cm^{-1}; ^{1}HNMR (400 MHz, DMSO-D_6): δ 5.6 (s, 2H), 7.08 (t, $J=8.8$ Hz, 1H), 7.18 (d, $J=2.4$ Hz, 1H), 7.38 (d, $J=8.8$ Hz, 1H), 7.75 (d, J = 2.8 Hz, 1H), 11.8 (s, 1H); ^{1}HNMR-D_2O exchange (400 MHz, DMSO-D_6): δ7.13 (d, $J=8$ Hz, 1H), 7.17 (s, 1H), 7.41 (d, $J=7.6$ Hz, 1H), 7.78 (s,1H); ^{13}CNMR (100 MHz, DMSO-D_6): δ 106.58, 122.61, 124.11, 128.52, 140.10, 140.75, 148.34, 161.13; HRMS (ESI): *m/z* calcd. for $C_8H_7N_3O$ $[M+H]^+$: 162.06, found: 162.0662; Anal calcd. for $C_8H_7N_3O$: C: 59.62; H: 4.38; N: 26.07%; found C: 59.60; H: 4.36; N: 26.05%; anti-TB activity MIC (H37Rv assay): 100 µg/ml.

Compound (4): 3-(2-morpholinoacetamido)-*N*-(3,4-dihydro-4-oxo-quinazolin-5-yl) benzamide

Highly hygroscopic solid, Yield: 50%; IR (KBR): 1109, 1444, 1607, 1663, 2860, 2919 cm^{-1}; ^{1}HNMR (400 MHz, DMSO-D_6): 1.25 (d, $J=6.4$ Hz, 5H), 1.99 (s, 2H), 2.70 (s, 1H), 3.14 (s, 3H), 7.09 (d, $J=7.6$ Hz, 1H), 7.40 (m, 3H), 7.52 (d, $J=8.4$ Hz, 1H), 7.70 (d, $J=8$ Hz, 1H), 7.76 (d, $J=6.4$ Hz, 1H), 7.85 (d, $J=8.4$ Hz, 1H), 9.90 (s, 1H); ^{13}CNMR (100 MHz, DMSO-D_6): δ 169.30, 168.88, 143.34, 139.15, 136.43, 129.29, 128.13, 125.89, 124.05, 122.27, 120.95, 119.11, 110.64, 66.55, 62.47, 60.24, 53.81, 21.56, 17.93, 14.54, 12.98; HRMS (ESI): *m/z* calcd. for $C_{21}H_{21}N_5O_4$ $[M+H]^+$: 408.16, found: 408.1672; Anal calcd. for $C_{21}H_{21}N_5O_4$: C: 65.01; H: 5.46; N: 13.78; found C: 65.00; H: 5.44; N: 13.76%; anti-TB activity MIC (H37Rv assay): 100 µg/ml.

Conclusion

In the present study, we studied MmaA1, a protein involved in the maturation of mycolic acids needed for cell wall synthesis of *Mycobacterium tuberculosis*, using structure-based drug design techniques. The 3-D model of the protein was built using Modeller and validated using Ramachandran plot, Verify_3D and ProSA. Active site of the MmaA1 protein was identified using CASTp, SiteMap and protein ligand docking. Virtual screening was performed using Schrodinger suite, and 141 docked complexes were obtained. The top 10 molecules prioritised based on Glide docking score are reported in this study. The residues ASP 19, TRP 30, TYR 32, GLY 71, TRP 74, GLY 76, ALA 77 and PHE 135 of the MmaA1 protein have shown important binding interactions with the ligands. ADME properties of the molecules were calculated using QikProp module of Schrodinger suite. All the top 10 molecules obey Lipinski's rule of five, Jorgensen rule of three and various other important pharmacokinetic parameters. In the present study, we have reported the synthesis of 3-(2-morpholinoacetamido)-*N*-(3,4-dihydro-4-oxoquinazolin-7-yl) benzamide and its intermediates. The synthesised compound and its intermediate compounds have shown good micromolar anti-tubercular activity. These results along with acceptable ADME properties suggest this class of compounds may furnish candidates for future development of novel anti-TB drugs.

Acknowledgements The author HV acknowledges Department of Science and Technology (DST), Government of India, for financial support under the Women Scientist Scheme (WOS-A) vide reference no. SR/WOS-A/CS-1031/2014. The authors HV, VM, KKM, RV, RM and UV acknowledge the Principal and Head, Department of Chemistry, University College of Sciences, Osmania University, Hyderabad, India,

for providing the facilities to carry out this work. The authors HV and MMK acknowledge the Principal, AU College of Pharmaceutical Sciences, Andhra University, Visakhapatnam, India, for providing the facilities to carry out this work.

Compliance with ethical standards

Conflict of interest The authors declare that they have no conflict of interest.

References

1. World Health Organisation (2019) Global tuberculosis. https://apps.who.int/iris/handle/10665/274453 Accessed on 10 Feb 2020
2. WHO Global Tuberculosis Programme (2002) An expanded DOTS framework for effective Tuberculosis control. Stop TB communicable diseases. Geneva: World Health Organisation. WHO/CDS/TB/2002.297
3. Osborne R (2013) First novel anti-tuberculosis drug in 40 years. Nat Biotech 31(2):89–90. https://doi.org/10.1038/nbt0213-89
4. Li Y, Sun F, Zhang W (2019) Bedaquiline and delamanid in the treatment of multi drug resistant tuberculosis: promising but challenging. Drug Dev Res 80:98–105. https://doi.org/10.1002/ddr.21498
5. Villemagne B, Crauste C, Flipo M, Baulard AR, Willand N (2012) Tuberculosis: the drug development pipeline at a glance. Eur J Med Chem 51:1–16. https://doi.org/10.1016/j.ejmech.2012.02.033
6. Marais BJ (2013) History of tuberculosis and drug resistance. New Engl J Med 386(1):88–90. https://doi.org/10.1056/NEJMc1212308
7. Nagasree KP, Murali Krishna Kumar M (2016) Chapter 1 In: Antitubercular drug therapy—past, present and future. Science Publishing Group, New York, pp 1–14. ISBN: 978-1-940366-14-2
8. Companico Andre, Moreira R, Lopes RF (2018) Drug discovery in tuberculosis: new drug targets and antimycobacterial agents. Eur J Med Chem 150:525–545. https://doi.org/10.1016/j.ejmech.2018.03.020
9. Brennan PJ (2003) Structure, function and biogenesis of the cell wall of *mycobacterium tuberculosis*. Tuberculosis 83:91–97. https://doi.org/10.1016/S1472-9792(02)00089-6
10. Marrakchi H, Laneelle MA, Daffe M (2014) Mycolic acids: structures, biosynthesis and beyond. Chem Biol 21(1):67–85. https://doi.org/10.1016/j.chembiol.2013.11.011
11. Barry CE III, Lee RE, Mdluli K, Sampson AE, Schroeder BG, Slayden RA, Yuan Y (1998) Mycolic acids: structure, biosynthesis and physiological functions. Prog Lipid Res 37:143–179. https://doi.org/10.1016/s0163-7827(98)00008-3
12. Asselineau C, Asselineau J, Laneellee G, Laneelle MA (2002) The biosynthesis of mycolic acids by Mycobacteria: current and alternative hypotheses. Prog Lipid Res 41(6):501–523. https://doi.org/10.1016/s0163-7827(02)00008-5
13. Arora P, Goyal A, Natarajan VT, Rajakumara E, Verma P, Gupta R, Yousuf M, Trivedi OA, Mohanty D, Tyagi A, Sankaranarayan R, Gokhale RS (2009) Mechanistic and functional insights into fatty acid activation in *mycobacterium tuberculosis*. Nat Chem Biol 5:166–173. https://doi.org/10.1038/nchembio.143
14. Yuan Y, Mead D, Schroeder BG, Zhu Y, Barry CE III (1998) The biosynthesis of mycolic acids in *mycobacterium tuberculosis*. Enzymatic methy(lene) transfer to acyl carrier protein bound meromycolic acid in vitro. J Biol Chem 273(33):21282–21290. https://doi.org/10.1074/jbc.273.33.21282
15. Takayama K, Wang C, Besra GS (2005) Pathway to synthesis and processing of mycolic acids in *mycobacterium tuberculosis*. Clin Microbiol Rev 18(1):81–101. https://doi.org/10.1128/cmr.18.1.81-101.2005
16. Yuan Y, Crane DC, Musser JM, Sreevatsan S, Barry CE III (1997) MMAS-1, the branch point between cis and trans cyclopropane ring containing oxygenated mycolates in *mycobacterium tuberculosis*. J Biol Chem 272(15):10041–10049. https://doi.org/10.1074/jbc.272.15.10041
17. Brossier F, Veziris N, Truffot-Pernot C, Jarlier V, Sougakoff W (2011) Molecular investigation of resistance to the anti tuberculosis drug Ethionamide in multidrug-resistant clinical isolates of *mycobacterium tuberculosis*. Anti Microb Agent Chemother 55(1):355–360. https://doi.org/10.1128/AAC.01030-10
18. Cade CE, Dlouhy AC, Medzihradszky KF, Sala-Castillo SP, Ghiladi RA (2010) Isoniazid-resistance conferring mutations in *mycobacterium tuberculosis* KatG: catalase, peroxidise and INH-NADH adduct formation activities. Prot Sci 9(3):458–474. https://doi.org/10.1002/pro.324
19. Gasteiger E, Gattiker A, Hoogland C, Ivanyi I, Appel RD, Bairoch A (2003) Expasy: the proteomics server for in-depth protein knowledge and analysis. Nucleic Acids Res 31:3784–3788. https://doi.org/10.1093/nar/gkg563
20. Berman HM, Westbrook J, Feng Z, Gilliland G, Bhat TN, Weissig H, Shindyalov IN, Bourne PE (2000) The protein data bank. Nucleic Acids Res 28(1):235–242. https://doi.org/10.1093/nar/28.1.235
21. Altschul SF, Gish W, Miller W, Myers EW, Lipman DJ (1990) Basic local alignment search tool. J Mol Biol 215:403–410. https://doi.org/10.1016/S0022-2836(05)80360-2
22. Christian C, Jonathan DB, Geoffrey JB (2008) The Jpred3 secondary structure prediction server. Nucleic Acids Res 36:197–201. https://doi.org/10.1093/nar/gkn238
23. Thompson JD, Higgins DG, Gibson TJ (1994) ClustalW: improving the sensitivity of sequence alignment through sequence weighting, position—specific gap penalties and weight matrix choice. Nucleic Acids Res 22:4673–4680. https://doi.org/10.1093/nar/22.22.4673
24. Webb B, Sali A (2014) Comparative protein structure modeling using Modeller. Curr Protoc Bioinfo 5(6):1–32. https://doi.org/10.1002/0471250953.bi0506s47
25. Laskowski RA, MacArthur MW, Moss DS, Thornton JM (1993) PROCHECK: a program to check the stereochemical quality of protein structures. J Appl Crystallogr 26:283–291. https://doi.org/10.1107/S0021889892009944
26. Kamy Z, Eisenberg D (1994) The three dimensional profile method using residue preference as a continuous function of residue environment. Prot Sci 3:687–695. https://doi.org/10.1002/pro.5560030416
27. Wiedersten M, Sippl MJ (2007) ProSA-web: interactive web service for the recognition of errors in three-dimensional structures of proteins. Nucleic Acids Res 35:407–441. https://doi.org/10.1093/nar/gkm290
28. Sheik SS, Sundararajan P, Hussain ASZ, Sekar KK (2002) Ramachandran plot on the web. Bioinformatics 18(11):1548–1549. https://doi.org/10.1093/bioinformatics/18.11.1548
29. Carrascoza F, Zaric S, Silaghi-Dumitrescu R (2014) Computational study of protein secondary structure elements: Ramachandran plots revisited. J Mol Graph Model 50:125–133. https://doi.org/10.1016/j.jmgm.2014.04.001
30. Dundas J, Ouyang Z, Tseng J (2006) CASTp: Computed atlas of surface topography of proteins with structural and topographical mapping of functionally annotated residues. Nucleic Acids Res 34:116–118. https://doi.org/10.1093/nar/gkl282

31. Halgren T (2007) New method for fast and accurate binding site identification and analysis. Chem Biol Drug Des 69:146–148. https://doi.org/10.1111/j.1747-0285.2007.00483.x
32. Duhovny DS, Inbar Y, Nussinov R, Wolfson HJ (2005) Patchdock and SymmDock: servers for rigid and symmetric Docking. Nucleic Acids Res 33:363–367. https://doi.org/10.1093/nar/gki481
33. Julien V, Fabienne B, Fanny B (2009) *S*-adenosyl-*N*-decylaminoethyl, a potent bisubstrate inhibitor of mycobacterium tuberculosis mycolic acid methyl transferases. J Biol Chem 284(29):19321–19330. https://doi.org/10.1074/jbc.M809599200
34. Shoichet BK (2004) Virtual screening of chemical libraries. Nature 432:862–865. https://doi.org/10.1038/nature03197
35. Kitchen DB (2004) Docking and scoring in virtual screening for drug discovery: methods and applications. Nat Rev Drug Discov 3:935–949. https://doi.org/10.1038/nrd1549
36. Friesner RA, Banks JL, Murphy RB, Halgren TA, Klicic JJ, Mainz DT, Repasky MP, Knoll EH, Shelley M, Perry JK, Shaw DE, Francis P, Shenkin PS (2004) Glide: a new approach for rapid, accurate docking and scoring. Method and assessment of docking accuracy. J Med Chem 47(7):1739–1749. https://doi.org/10.1021/jm0306430
37. Jorgensen WL, Maxwell DS, Tirado-Rives J (1996) Development and testing of the OPLS All-Atom force field on conformational energetics and properties of organic liquids. J Am Chem Soc 118:11225–11236. https://doi.org/10.1021/ja9621760
38. Kaminski GA, Friesner RA, Tirado-Rives J, Jorgensen WL (2001) Evaluation and reparametrization of the OPLS-AA force field for proteins via comparison with accurate quantum chemical calculations on peptides. J Phys Chem B 105(28):6474–6487. https://doi.org/10.1021/jp003919d
39. LigPrep, version 2.4 (2010) Schrodinger, LLC, New York, NY
40. Friesner RA, Murphy RB, Repasky MP, Frye LL, Greenwood JR, Halgren TA, Sanschagrin PC, Mainz DT (2006) Extra precision glide: docking and scoring incorporating a model of hydrophobic enclosure for protein–ligand complexes. J Med Chem 49:6177–6196. https://doi.org/10.1021/jm051256o
41. Sean E, Waller CL, Swaan PW, Cruciani G, Wrighton SA, Wikel JH (2000) Progress in predicting human ADME parameters in silico. J Pharmacol Tox Methods 44(1):251–272. https://doi.org/10.1016/s1056-8719(00)00109-x
42. Valerio LG Jr (2009) In silico toxicology for the pharmaceutical sciences. Toxicol Appl Pharmacol 241:356–370. https://doi.org/10.1016/j.taap.2009.08.022
43. QikProp (2010) Schrodinger, LLC, New York, NY
44. Tahlan S, Ramasamy K, Lim SM, Shah SAA, Mani V, Narasimhan B (2018) Design, synthesis and therapeutic potential of 3-(2-(1H-benzo[d]imidazol-2-ylthio)acetamido)-*N*-(substituted phenyl) benzamide analogues. Chem Cent J 12(1):139. https://doi.org/10.1186/s13065-018-0513-3
45. Wayland EN, Rieke RD (1962) New synthetic route to 6-nitroisatin via nitration of 3-indole aldehyde. J Org Chem 27(6):2250–2252. https://doi.org/10.1021/jo01053a529
46. Gabriel FR, Silva BV, Martinez ST, Pinto AC (2015) Anthranilic acids from isatin: an efficient, versatile and environmentally friendly method. Ann Acad Braz Sci 87(3):1525–1529. https://doi.org/10.1590/0001-3765201520140289
47. Sharma GVR, Robert AR (2012) Synthetic strategies to Quinazolinones. Int J Adv Pharm Biol Chem 1(3):337–341 **ISSN: 2277-4688**
48. Valeur E, Bradley M (2009) Amide bond formation: beyond the myth of coupling reagents. Chem Soc Rev 38(2):38606–38631. https://doi.org/10.1039/B701677H
49. Nakayama GR, Caton MC, Nova MP, Parandoosh Z (1997) Assessment of the Alamar Blue assay for cellular growth and viability in vitro. J Immunol Methods 204(2):205–208. https://doi.org/10.1016/s0022-1759(97)00043-4
50. Daisy Vanitha J, Paramasivan CN (2004) Evaluation of Microplate Alamar Blue assay for drug susceptibility testing of *Mycobacterium avium* complex isolates. Diagn Microbiol Infect Dis 49:179–182. https://doi.org/10.1016/j.diagmicrobio.2004.04.003
51. Laskowsky RA, Watson DJ, Thornton MJ (2005) ProFunc: a server for predicting protein function from 3D structure. Nucleic Acids Res 33:89–93. https://doi.org/10.1093/nar/gki414
52. The PyMOL Molecular Graphics System, Version 2.0, Schrodinger LLC
53. Ramakrishna D, Ramasree D, Bhargavi K, Vishwanath R, Shantiprada V, Rajender V, Uma V (2016) Suppressor of cytokine signalling-3 as a drug target for type2 diabetes mellitus: a structure guided approach. Chem Select 1:2502–2514. https://doi.org/10.1002/jmr.2706
54. Ramesh M, Rajender V, Hymavathi V, Kiran Kumar M, Vasavi M, Uma V (2017) Identification of small molecular ligands as potent inhibitors of fatty acid metabolism in *Mycobacterium tuberculosis*. J Mol Struct 1150:227–241. https://doi.org/10.1016/j.molstruc.2017.08.090
55. Rajender V, Kiran Kumar M, Vasavi M, Ramasree D, Hymavathi V, Ramesh M, Uma V (2018) Identification of small molecular inhibitors for efflux protein Rv2688c of *Mycobacterium tuberculosis*. Biotechnol Appl Biochem 65(4):608–621. https://doi.org/10.1002/bab.1647
56. Accelrys Discovery Studio Visualiser, version 3.5